



# Mixing state of oxalic acid containing particles in the rural area of Pearl River Delta, China: implications for the formation mechanism of oxalic acid

Chunlei Cheng<sup>1,2</sup>, Mei Li<sup>1,2</sup>, Chak K. Chan<sup>3</sup>, Haijie Tong<sup>4</sup>, Changhong Chen<sup>5</sup>, Duohong Chen<sup>6</sup>, Dui Wu<sup>1,2</sup>, Lei Li<sup>1,2</sup>, Cheng Wu<sup>1,2</sup>, Peng Cheng<sup>1,2</sup>, Wei Gao<sup>1,2</sup>, Zhengxu Huang<sup>1,2</sup>, Xue Li<sup>1,2</sup>, Zhijuan Zhang<sup>1,2</sup>, Zhong Fu<sup>7</sup>, Yanru Bi<sup>7</sup>, and Zhen Zhou<sup>1,2</sup>

<sup>1</sup>Institute of Mass Spectrometer and Atmospheric Environment, Jinan University, Guangzhou 510632, China

<sup>2</sup>Guangdong Provincial Engineering Research Center for on-line source apportionment system of air pollution, Guangzhou 510632, China

<sup>3</sup>School of Energy and Environment, City University of Hong Kong, Hong Kong, China

<sup>4</sup>Max Planck Institute for Chemistry, Multiphase Chemistry Department, Hahn-Meitner-Weg 1, 55128 Mainz, Germany

<sup>5</sup>State of Environmental Protection Key Laboratory of the formation and prevention of urban air pollution complex, Shanghai Academy of Environmental Sciences, Shanghai 200233, China

<sup>6</sup>State Environmental Protection Key Laboratory of Regional Air Quality Monitoring, Guangdong Environmental Monitoring Center, Guangzhou, 510308, China

<sup>7</sup>Guangzhou Hexin Analytical Instrument Limited Company, Guangzhou 510530, China

Correspondence to: Mei Li (limei2007@163.com) and Zhen Zhou (zhouzhen@gig.ac.cn)

Received: 1 December 2016 – Discussion started: 21 December 2016

Revised: 6 July 2017 – Accepted: 10 July 2017 – Published: 8 August 2017

**Abstract.** The formation of oxalic acid and its mixing state in atmospheric particulate matter (PM) were studied using a single-particle aerosol mass spectrometer (SPAMS) in the summer and winter of 2014 in Heshan, a supersite in the rural area of the Pearl River Delta (PRD) region in China. Oxalic-acid-containing particles accounted for 2.5 and 2.7 % in total detected ambient particles in summer and winter, respectively. Oxalic acid was measured in particles classified as elemental carbon (EC), organic carbon (OC), elemental and organic carbon (ECOC), biomass burning (BB), heavy metal (HM), secondary (Sec), sodium-potassium (NaK), and dust. Oxalic acid was found predominantly mixing with sulfate and nitrate during the whole sampling period, likely due to aqueous-phase reactions. In summer, oxalic-acid-containing particle number and ozone concentration followed a very similar trend, which may reflect the significant contribution of photochemical reactions to oxalic acid formation. The HM particles were the most abundant oxalic acid particles in summer and the diurnal variations in peak area of iron and oxalic acid show opposite trends, which suggests a possible loss of oxalic acid through the photolysis of iron oxalato-

complexes during the strong photochemical activity period. In wintertime, carbonaceous particles contained a substantial amount of oxalic acid as well as abundant carbon clusters and BB markers. The general existence of nitric acid in oxalic-acid-containing particles indicates an acidic environment during the formation process of oxalic acid. The peak areas of nitrate, sulfate and oxalic had similar temporal change in the carbonaceous type oxalic acid particles, and the organosulfate-containing oxalic acid particles correlated well with total oxalic acid particles during the haze episode, which suggests that the formation of oxalic acid is closely associated with the oxidation of organic precursors in the aqueous phase.

## 1 Introduction

Organic aerosol, typically a large fraction of fine particles, contains thousands or more of organic compounds and contributes to visibility reduction, photochemical smog, climate

change and adverse health effects (Novakov and Penner, 1993; Goldstein and Galbally, 2007; Jimenez et al., 2009; Pöschl and Shiraiwa, 2015). A significant component of organic aerosol is secondary organic aerosol (SOA) formed from the gas-phase oxidation of volatile organic compounds (VOCs) followed by partitioning of products into particles or from heterogeneous reactions of VOCs with particles (Hallquist et al., 2009; Zhang et al., 2015). Dicarboxylic acids (DCAs) are abundant and ubiquitous constituents in SOA and can be effective tracers for the oxidative processes leading to the formation of SOA (Kawamura and Ikushima, 1993; Ervens et al., 2011; Wang et al., 2012; Cheng et al., 2013). DCAs normally have high water solubility and low vapor pressure. Thus, they play important roles in controlling the hygroscopic properties of organic aerosols (Prenni et al., 2003; Ma et al., 2013) and activating cloud condensation nuclei (Booth et al., 2009). The primary emissions of DCAs from anthropogenic sources in urban areas are minor (Huang and Yu, 2007; Stone et al., 2010), and they are mainly derived from secondary oxidation of VOCs and subsequent intermediates (Ho et al., 2010; Myriokefalitakis et al., 2011). High concentrations of DCAs have been observed in biomass burning plumes (Kundu et al., 2010; Kawamura et al., 2013), with more than 70 % of DCAs produced from photochemical oxidation of water-soluble organic compounds, and only a small contribution from direct biomass burning (BB) emission (van Pinxteren et al., 2014).

The production of DCAs through photochemical reactions has been reported in many field studies via the analysis of the diurnal and seasonal variations in DCA (dicarboxylic acid) (Kawamura and Ikushima, 1993; Kawamura and Yasui, 2005; Aggarwal and Kawamura, 2008; Pavuluri et al., 2010; Ho et al., 2011; Wang et al., 2017), but the mechanism of DCA formation is still not well understood. Oxalic acid is usually the most abundant DCA observed in the field (Kawamura et al., 2004, 2010; Ho et al., 2007). A number of ground-based and airborne field studies have found a close correlation between oxalic acid and sulfate in ambient particles and cloud droplets, relating aqueous-phase chemistry to the formation of oxalic acid in aerosols and cloud droplets (Yao et al., 2002, 2003; Yu et al., 2005; Sorooshian et al., 2006, 2007a, b; Miyazaki et al., 2009; Wonschuetz et al., 2012; Wang et al., 2016). In recent years, several model and laboratory studies have suggested that the aqueous-phase oxidation of highly water-soluble organics like glyoxal, methylglyoxal and glyoxylic acid can efficiently produce oxalic acid in aerosol particles and cloud droplets (Lim et al., 2010; Myriokefalitakis et al., 2011; Ervens et al., 2014; Yu et al., 2014; McNeill, 2015). Recent stable carbon isotope studies and field observations have also suggested that oxalic acid forms through aqueous-phase reactions (Wang et al., 2012; Cheng et al., 2015). However, the formation process of oxalic acid in ambient aerosols is still associated with great uncertainty due to the oxidation rates of precursors and ox-

idant levels in photochemistry and aqueous-phase chemistry, which needs to be further studied.

Online measurements of the size distribution of oxalic-acid-containing particles and the mixing state of oxalic acid with other compounds in aerosols are useful for examining the formation and evolution of oxalic acid and SOA particles. Sullivan and Prather (2007) investigated the diurnal cycle and mixing state of DCA-containing particles in Asian aerosol outflow using aerosol time-of-flight mass spectrometry (ATOFMS) and proposed the formation of DCA on Asian dust. In addition, Yang et al. (2009) measured oxalic acid particles in Shanghai and proposed that in-cloud processes and heterogeneous reactions on hydrated aerosols contributed to the formation of oxalic acid (Yang et al., 2009). While the formation mechanism of oxalic acid, especially in urban areas, is still not clear, online measurements of the mixing state of oxalic acid provide a powerful tool to better understand the formation of oxalic acid in aerosol particles and cloud droplets.

The Pearl River Delta (PRD) region has distinct meteorological seasonality under the influence of the Asian monsoon system, which brings air from the ocean in spring and summer and carries polluted air from northern China in autumn and winter. Strong photochemical activity occurs in summer under the condition of high temperature and relative humidity, and in winter high loadings of particles from northern cities are favorable for the occurrence of haze episodes (Bi et al., 2011; Zhang et al., 2013, 2014). Here we present the seasonal field measurements of the mixing state of oxalic-acid-containing particles using a single-particle aerosol mass spectrometer (SPAMS) at a rural supersite of the PRD region. The seasonal characteristics of oxalic acid particles and mixing state with secondary species were investigated to explore the formation mechanisms of oxalic acid and aging process of SOA.

## 2 Methods

### 2.1 Aerosol sampling

Particles were sampled using a SPAMS at the Guangdong atmospheric supersite (22.73° N, 112.93° E), a rural site at Heshan city (Fig. S1 in the Supplement). The supersite is surrounded by farmland and villages, with no local industrial or traffic emissions. Ambient aerosols were sampled using the SPAMS through a 2.5 m long copper tube with 0.5 m of the sampling inlet located above the top of the building. The measurement period was from 18 July to 1 August in 2014 and from 27 January to 8 February in 2015. Real-time PM<sub>2.5</sub> mass concentration was simultaneously measured by a TEOM monitor (series 1405, Thermo Scientific), and hourly concentrations of O<sub>3</sub> were measured by an O<sub>3</sub> analyzer (model 49i, Thermo Scientific). The local meteorological data including temperature, relative humidity and vis-

ibility were measured on the rooftop of the building. The average temperature during the field study was 29.5 °C in summer and 14.1 °C in winter and the average relative humidity was 71.7 and 63 % in summer and winter, respectively.

## 2.2 SPAMS

Real-time measurements of single atmospheric particles were used by Prather and co-workers in the 1990s using aerosol time-of-flight mass spectrometry (ATOFMS) (Prather et al., 1994; Noble and Prather, 1996). Based on the same principle, the SPAMS developed by Guangzhou Hexin Analytical Company was applied to field measurements of single particles in the current work. The details of the SPAMS system were introduced previously (Li et al., 2011). Briefly, aerosol particles are sampled into the vacuum pumped aerodynamic lens of the SPAMS through an electro-spark-machined 80 µm critical orifice at a flow rate of 75 mL min<sup>-1</sup>. The individual particles with terminal velocity are introduced to the sizing region. The velocity of each single-particle is detected by two continuous laser beams (diode Nd:YAG, 532 nm) with a space of 6 cm. The velocity is then used to calculate the single particle aerodynamic diameter and provide the precise timing of the firing of a 266 nm laser used to induce desorption and ionization (Nd:YAG laser, 266 nm). The energy of the desorption-ionization 266 nm laser was 0.6 mJ and the power density was kept at about  $1.06 \times 10^8$  W cm<sup>-2</sup> during both sampling periods. The 266 nm laser generates positive and negative ions that are detected by a Z-shaped bipolar time-of-flight mass spectrometer. The size range of the detected single particles is 0.2 to 2 µm. Polystyrene latex spheres (nanosphere size standards, Duke Scientific Corp., Palo Alto) of 0.22–2.0 µm diameter were used for size calibration.

## 2.3 Data analysis

The size and chemical composition of single particles detected by SPAMS were analyzed using the Computational Continuation Core (COCO) toolkit based on the MATLAB software. Particles were clustered into several groups using the neural network algorithm (ART-2a) to group particles into clusters with similar mass spectrum features. The ART-2a parameters used in this work were set to a vigilance factor of 0.8, a learning rate of 0.05 and a maximum of 20 iterations. We collected 516 679 and 767 986 particles with both positive and negative mass spectra in summer and winter, respectively. A standard solution of oxalic acid was prepared with pure oxalic acid (H<sub>2</sub>C<sub>2</sub>O<sub>4</sub>, purity: 99.99 %, Aladdin Industrial Corporation) and atomized to aerosols. After drying through two silica gel diffusion driers, pure oxalic acid particles were directly introduced into the SPAMS. The positive and negative mass spectra of oxalic acid are shown in Fig. S2. Based on the mass spectra of pure oxalic acid and previous ambient measurements using ATOFMS (Silva and Prather,

2000; Sullivan and Prather, 2007; Yang et al., 2009), HC<sub>2</sub>O<sub>4</sub><sup>-</sup> ( $m/z$  –89) is selected as the ion peak for oxalic acid containing particles. In this work, oxalic acid particles are identified if the peak area of  $m/z$  –89 was larger than 0.5 % of the total signal in the mass spectrum. With this threshold, 13 109 and 20 504 of oxalic-acid-containing particles were obtained in summer and winter separately, accounting for 2.5 and 2.7 % of the total detected particles. The percentage of oxalic-acid-containing particles in total particles in this work was comparable to the reported value in the urban area of Shanghai (3.4 %) (Yang et al., 2009). However, these percentages are in general much lower than those reported in cleaner environments such as the western Pacific Ocean where oxalic acid was found in up to 1–40 % of total particles due to little anthropogenic influences (Sullivan and Prather, 2007).

The oxalic acid containing particles are classified into eight types in the following order: elemental carbon (EC), organic carbon (OC), elemental and organic carbon (ECOC), BB, heavy metal (HM), secondary (Sec), sodium-potassium (NaK) and dust. Different types of particles are identified according to characteristic ion markers and dominant chemical species (Table S1 in the Supplement): (1) particles containing abundant carbon clusters like  $\pm 12[\text{C}]^{+/-}$ ,  $\pm 24[\text{C}_2]^{+/-}$  and  $\pm 36[\text{C}_3]^{+/-}$  with a relative peak area of more than 0.5 % are classified as EC type; (2) any remaining particles containing abundant signals of  $27[\text{C}_2\text{H}_3]^+$ ,  $43[\text{C}_2\text{H}_3\text{O}]^+$  and hydrocarbon clusters with a relative peak area of more than 0.5 % are classified as OC type; (3) any remaining particles containing signals of  $\pm 12[\text{C}]^{+/-}$ ,  $\pm 24[\text{C}_2]^{+/-}$ ,  $37[\text{C}_3\text{H}]^+$  and  $43[\text{C}_2\text{H}_3\text{O}]^+$  with a relative peak area of more than 0.5 % are classified as ECOC type; (4) any remaining particles containing abundant signals of  $39[\text{K}]^+$  (peak area > 1500) with a relative peak area of  $-59[\text{C}_2\text{H}_3\text{O}_2]^-$  and  $-73[\text{C}_3\text{H}_5\text{O}_2]^-$  of simultaneously more than 0.5 % are classified as BB type; (5) any remaining particles containing signals of  $55[\text{Mn}]^+$ ,  $56[\text{Fe}]^+$ ,  $63/65[\text{Cu}]^+$ ,  $64[\text{Zn}]^+$  and  $208[\text{Pb}]^+$  with a relative peak area of more than 0.5 % are classified as HM type; (6) any remaining particles containing abundant signals of  $18[\text{NH}_4]^+$  (peak area > 50),  $-62[\text{NO}_3]^-$  (peak area > 100) and  $-97[\text{HSO}_4]^-$  (peak area > 100) are classified as Sec type; (7) any remaining particles containing abundant signals of  $23[\text{Na}]^+$  (peak area > 1500) and related species are classified as NaK type; (8) any remaining particles containing signals of  $40[\text{Ca}]^+$ ,  $56[\text{CaO}]^+$  and related species are classified as dust type. The rules for oxalic acid particle classification in the current work have been reported in previous studies (Sullivan and Prather, 2007; Yang et al., 2009; Zhang et al., 2013; Li et al., 2014).

## 2.4 Inorganic ions and in situ pH (pH<sub>is</sub>)

Water-soluble inorganic ions and trace gases were determined by an online analyzer for monitoring aerosols and gases (MARGA, model ADI 2080, Applikon Analytical B. V. Corp., the Netherlands), with a PM<sub>2.5</sub> sampling inlet at

1 h resolution from 18 July to 1 August in 2014. The principle and instrumental design has been described in detail elsewhere (ten Brink et al., 2007; Du et al., 2011; Behera et al., 2013; Khezri et al., 2013). Standard solutions containing all detected ions were injected into MARGA before and after the field measurement. The liquid water content and the concentration of  $H^+$  in particles are calculated using the ISORROPIA II model (Nenes et al., 1998, 1999; Fountoukis and Nenes, 2007). We choose stable mode and reverse type in the ISORROPIA model to calculate the concentration of  $H^+$  and the liquid water content in this work. The in situ pH ( $pH_{is}$ ) of particles is calculated through the following equation:

$$pH_{is} = -\log \alpha_{H^+} = -\log (\gamma_{H^+} \times n_{H^+} \times 1000/V_a), \quad (1)$$

in which  $n_{H^+}$  is the concentration of  $H^+$  ( $\text{mol m}^{-3}$ ) and  $V_a$  is the volume concentration of the  $H_2O$  ( $\text{cm}^3 \text{m}^{-3}$ ), while  $\gamma_{H^+}$  is the activity coefficient of  $H^+$  (Xue et al., 2011; Cheng et al., 2015). The temporal variation in  $pH_{is}$  of ambient  $PM_{2.5}$  particles is presented in Fig. S3 and demonstrated that 97 % of particles were acidic in summer.

### 3 Results and discussion

#### 3.1 Seasonal variation in oxalic-acid-containing particles

The clustered 48 h back trajectories of air masses arriving in Heshan during the sampling period are shown in Fig. S4. In summer, air masses at 500 m levels above the ground were mainly from the ocean and rural areas with less influence of human activity, while in winter air masses were directly from the urban areas of Guangzhou and Foshan, indicating a strong influence from anthropogenic emissions. The temporal variations in the total detected particles and oxalic acid containing particles in summer and winter are shown in Fig. 1. The total particles had similar trends with the mass concentration of ambient  $PM_{2.5}$ , suggesting that the counts of total particles detected by SPAMS can be representative of  $PM_{2.5}$  mass concentration during the whole sampling period. The oxalic acid ( $C_2$ -containing) particles, in general, exhibited distinct diurnal peaks from 28 July to 1 August, while they showed different temporal trends in winter. The relative abundance of oxalic acid particles in all of the sampled particles ( $C_2$  / total ratio) had the same variation with the abundance of oxalic acid particles in summer, especially in the period of 28 July–1 August (Fig. 1). In winter, however, particle counts and relative abundance of oxalic acid had different temporal changes, except in 30 January and 5–8 February, when the count and relative abundance of oxalic acid particles simultaneously had a sudden increase.

The oxalic-acid-containing particles were clustered into eight groups, and they altogether accounted for 89.6 and 95.1 % of total oxalic acid particles in summer and winter, respectively. Table 1 shows that in summer HM particles con-

**Table 1.** Summary of major groups of oxalic-acid-containing particles in summer and winter in PRD, China.

Particle type	Summer (18 Jul–1 Aug 2014)		Winter (27 Jan–8 Feb 2015)	
	Count	Percentage, %	Count	Percentage, %
EC	1473	11.2	3161	15.4
ECOC	41	0.3	2233	10.9
OC	473	3.6	1922	9.4
BB	1702	13.0	4953	24.2
HM	4104	31.3	3124	15.2
Sec	2511	19.2	2192	10.7
NaK	303	2.3	17	0.1
Dust	1139	8.7	1888	9.2

Abbreviations of major particle types: elemental carbon (EC), elemental and organic carbon (ECOC), organic carbon (OC), biomass burning (BB), heavy metal (HM), secondary (Sec), sodium-potassium (NaK), and dust (Dust).

tributed 31.3 % to total oxalic acid particles, followed by Sec (19.2 %) and BB (13 %) particles. However, in winter BB particles were the most abundant and accounted for 24.2 % of the oxalic-acid-containing particles, followed by EC and HM particles. In addition, carbonaceous particles, including EC, OC, ECOC and BB, accounted for 28.1 % of oxalic acid particles in summer and 59.8 % in winter, indicating the different seasonal characteristics of oxalic acid particles. The temporal variations in eight groups of oxalic acid particles in summer and winter are illustrated in Fig. 1. In summer HM particles (orange color) and total oxalic acid particles exhibited similar diurnal patterns, suggesting a possible connection between the production of oxalic acid and the transition metals (e.g., Fe, Cu) (Zhou et al., 2015). Although Sec, BB and EC particles showed similar diurnal patterns with total oxalic acid particles, the concentrations of these types of particles were generally lower than HM particles. In winter, diurnal variation of oxalic acid particles was not obvious but a sharp increase, accompanied by the increase in BB, EC and Sec particles, was observed on 8 February.

The averaged positive and negative ion mass spectra of oxalic acid containing particles are shown in Fig. 2. The positive ion spectrum of oxalic acid particles in summer was characterized by high fractions of metal ion peaks, including  $23[Na]^+$ ,  $27[Al]^+$ ,  $39[K]^+$ ,  $55[Mn]^+$ ,  $56[Fe]^+$ ,  $63/65[Cu]^+$ ,  $64[Zn]^+$ , and  $208[Pb]^+$  and carbonaceous marker ions at  $m/z$   $27[C_2H_3]^+$ ,  $36[C_3]^+$ ,  $43[C_2H_3O/C_3H_7]^+$ , and  $48[C_4]^+$  (Fig. 2a). The negative ion spectrum of oxalic acid particles in summer was characterized by the strong intensity of secondary ions, including  $m/z$   $-46[NO_2]^-$ ,  $-62[NO_3]^-$ ,  $-79[PO_3]^-$ ,  $-80[SO_3]^-$ ,  $-96[SO_4]^-$ , and  $-97[HSO_4]^-$ , as well as carbon clusters of  $-24[C_2]^-$ ,  $-36[C_3]^-$ , and  $-48[C_4]^-$  and BB markers of  $-59[C_2H_3O_2]^-$  and  $-73[C_3H_5O_2]^-$  (Fig. 2b) (Zauscher et al., 2013). More carbonaceous clusters, i.e.,  $27[C_2H_3]^+$ ,  $29[C_2H_5]^+$ ,  $36[C_3]^+$ ,  $37[C_3H]^+$ ,  $43[C_2H_3O]^+$ ,  $48[C_4]^+$ ,  $51[C_4H_3]^+$ ,  $55[C_4H_7]^+$ ,  $60[C_5]^+$ ,  $63[C_5H_3]^+$ ,  $65[C_5H_5]^+$  and  $74[C_2H_2O_3]^+$ ,  $77[C_6H_5]^+$ , were observed in the posi-

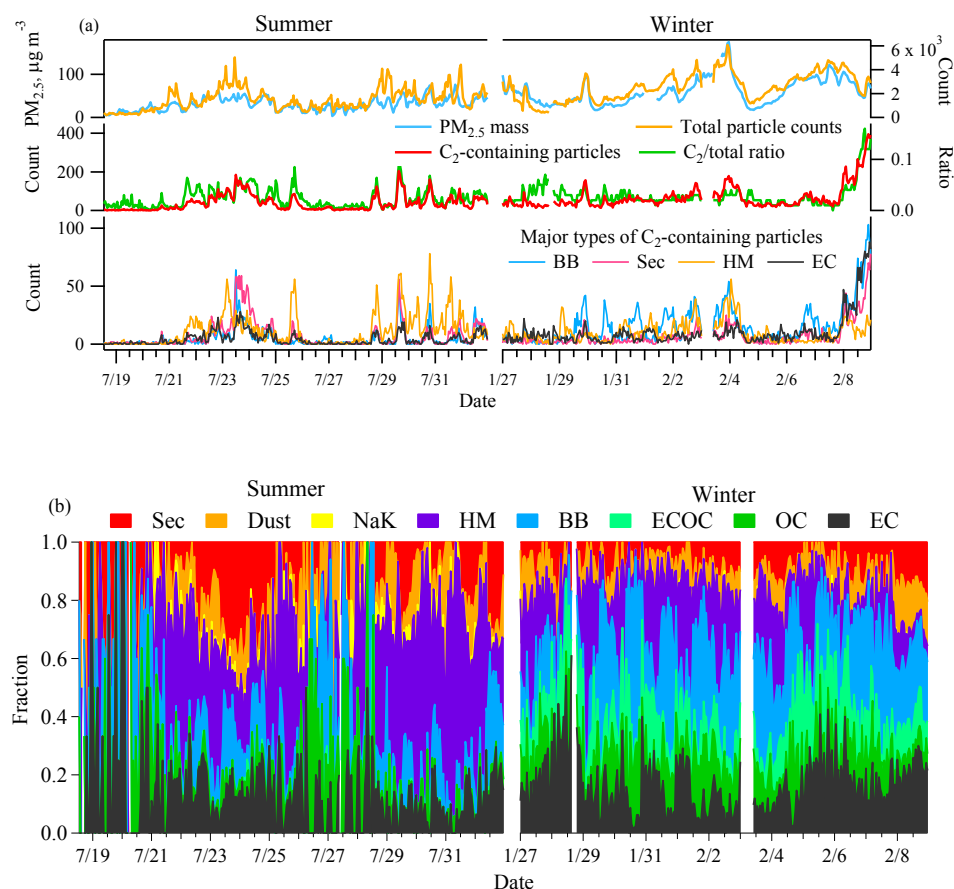


**Figure 1.** Temporal variations in total detected particles and oxalic-acid-containing particles during the whole sampling period in Heshan, China: **(a)** hourly variations in PM<sub>2.5</sub> mass concentration, total detected particle counts, oxalic acid containing particles, ratio of oxalic-acid-containing / total particles and major types of oxalic-acid-containing particles; **(b)** variation patterns of relative abundance of major types of oxalic-acid-containing particles.

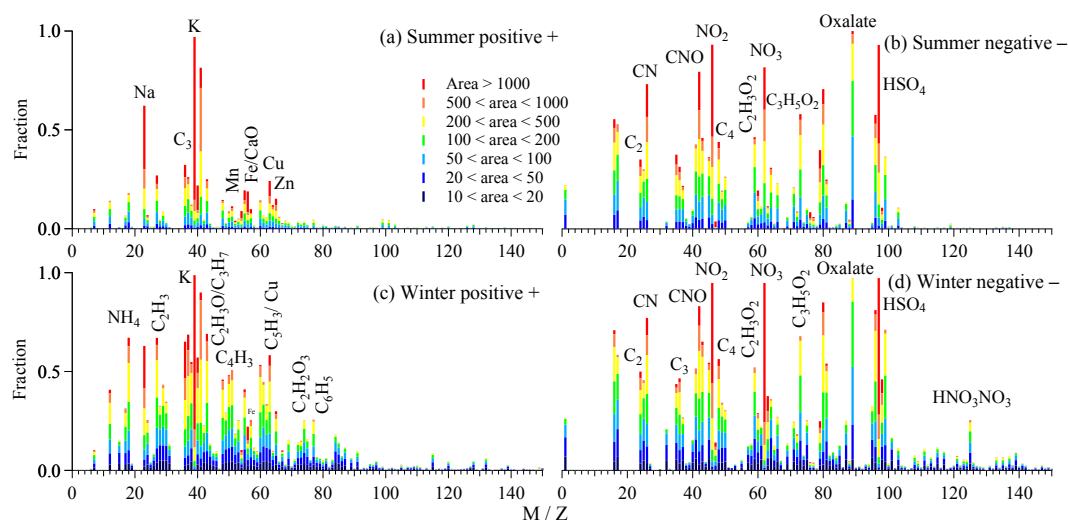


**Figure 2.** The averaged positive and negative ion mass spectra of oxalic-acid-containing particles is investigated in summer and winter: **(a)** summer positive, **(b)** summer negative, **(c)** winter positive and **(d)** winter negative. The color bars represent each peak area corresponding to a specific fraction in individual particles.

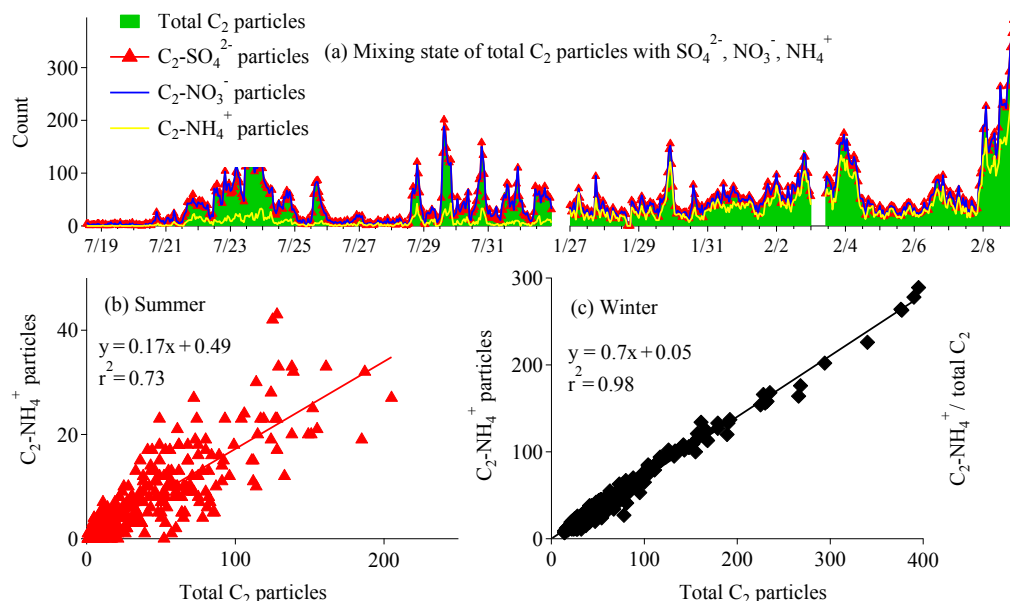


**Figure 3.** (a) Mixing state of oxalic acid with sulfate, nitrate and ammonium in oxalic-acid-containing particles; (b) linear correlation between NH<sub>4</sub><sup>+</sup>-containing oxalic acid particles and the total oxalic acid particles in summer; (c) linear correlation between NH<sub>4</sub><sup>+</sup>-containing oxalic acid particles and the total oxalic acid particles in winter. Abbreviations: C<sub>2</sub>-NH<sub>4</sub><sup>+</sup> represents the NH<sub>4</sub><sup>+</sup>-containing oxalic acid particles and C<sub>2</sub>-SO<sub>4</sub><sup>2-</sup> and C<sub>2</sub>-NO<sub>3</sub><sup>-</sup> follow the same pattern.

tive ion spectrum of oxalic acid particles in winter (Fig. 2c) than in summer. The negative ion spectrum of oxalic acid particles in winter (Fig. 2d) contained a large number of secondary ions, similar to those found in summer, and a more intense signal of nitric acid ( $-125[\text{HNO}_3\text{NO}_3]^-$ ), suggesting an acidic nature of oxalic acid particles in winter.

The mixing state of oxalic acid particles with sulfate, nitrate and ammonium (SNA) was investigated through the percentage of SNA-containing oxalic acid particles in total oxalic acid particles (Fig. 3). Oxalic acid was found to be internally mixed with sulfate and nitrate during both sampling periods with 93 and 94 % in summer respectively, and both with 98 % in winter (Fig. 3a). However, the NH<sub>4</sub><sup>+</sup>-containing oxalic acid particle (C<sub>2</sub>-NH<sub>4</sub><sup>+</sup>) only accounted for 18 % of total oxalic acid particles in summer but this fraction increased to 71 % in winter, and linear correlation between C<sub>2</sub>-NH<sub>4</sub><sup>+</sup> particles and total oxalic acid particles showed better linear regression ( $r^2 = 0.98$ ) in winter than summer, indicating a general mixing state of NH<sub>4</sub><sup>+</sup> with oxalic acid in winter. Aqueous-phase production of SO<sub>4</sub><sup>2-</sup> has been studied well and the linear correlation between oxalic acid and SO<sub>4</sub><sup>2-</sup> has been used to study the production of oxalic acid through aqueous-phase reactions (Yu et al., 2005; Miyazaki et al., 2009; Cheng et al., 2015). In our work, oxalic acid and C<sub>2</sub>-SO<sub>4</sub><sup>2-</sup> displayed good correlations in summer and winter (both  $r^2 = 0.99$ ), which suggests a common production route of oxalic acid and sulfate, likely aqueous-phase reactions.

Figure 4 shows the unscaled size-resolved number distributions of the eight types of oxalic acid particles. Oxalic acid mainly existed in 0.4 to 1.2 μm particles during the entire sampling period but exhibited different peak modes for each particle type in summer and winter. In summer, major types of oxalic acid particles showed distinct peak mode at different size diameters. EC and Sec particles peaked at 0.5 μm, followed by BB particles at 0.55 μm, then HM particles at 0.6 μm, and OC particles at 0.7 μm. The difference in peak mode suggests the possible different chemical evolution process for each type of oxalic-acid-containing particle. However, in winter, oxalic acid particles showed broader size distribution from 0.5 to 0.8 μm for all particle types. Oxalic acid particles of all types were generally larger in winter than summer, possibly due to condensation and coagulation of particles during aging of oxalic acid particles in winter.

### 3.2 Photochemical production of oxalic acid in summer

In summer oxalic acid particles showed peaks in the afternoon especially from 28 July to 1 August, which was in agreement with the variation pattern of the O<sub>3</sub> concentration (Fig. 5), indicating a strong association of oxalic acid formation with photochemical reactions. Malonic acid is another product of photochemical oxidation of organic compounds (Kawamura and Ikushima, 1993; Wang et al., 2012; Meng et al., 2013, 2014). In our campaign, malonic-acid-containing particles had diurnal trends similar to oxalic acid particles and O<sub>3</sub> concentration. As the dominant particle type, HM

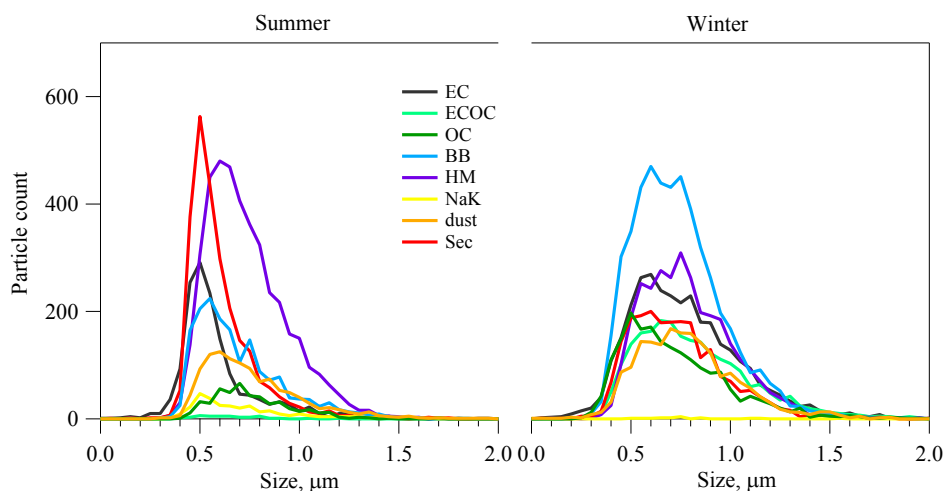


**Figure 4.** Unscaled size-resolved number distributions of major types of oxalic acid particles in summer and winter.

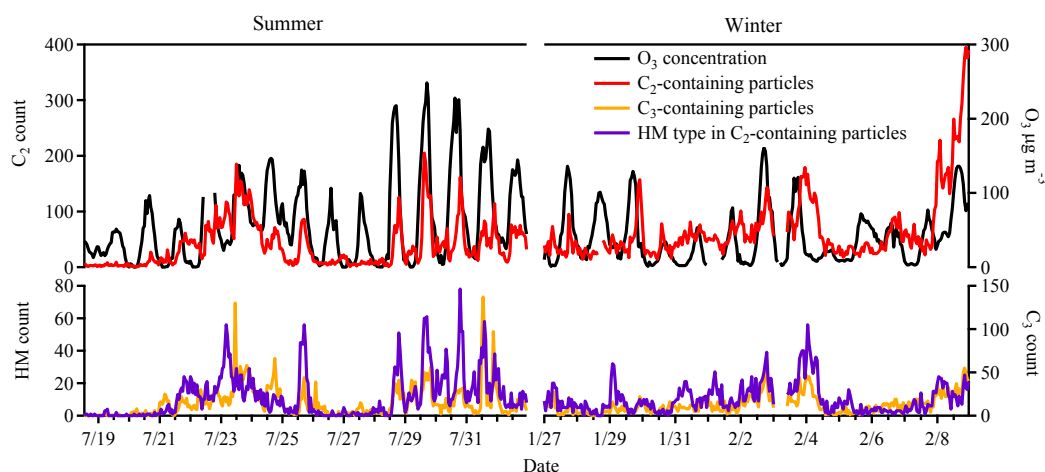


**Figure 5.** Temporal variations in  $O_3$  concentrations, oxalic acid particles, malonic acid particles and heavy metal oxalic acid particles during the entire sampling period in Heshan, China.

particles had variation patterns identical to total oxalic acid particles. They are characterized by highly abundant metal ion peaks like  $55[Mn]^+$ ,  $56[Fe]^+$ ,  $63/65[Cu]^+$ ,  $64[Zn]^+$  and  $208[Pb]^+$ , as well as secondary ion peaks of  $-46[NO_2]^-$ ,  $-62[NO_3]^-$ ,  $-80[SO_3]^-$ ,  $-96[SO_4]^-$  and  $-97[HSO_4]^-$  in the negative spectrum in summer (Fig. 6). In order to investigate the photochemical formation of oxalic acid in summer, the diurnal variations in  $O_3$ , oxalic acid particles, HM particles and  $pH_{is}$  of ambient particles averaged from 28 July to 1 August 2014 are shown in Fig. 7. The concentration of  $O_3$  increased after 09:00 and peaked at 17:00 (all times hereafter in Beijing time, UTC + 8), while oxalic acid particles and HM particles both increased after 10:00 and showed two peaks at 15:00 and 19:00. The  $pH_{is}$  of ambient particles ranging from  $-1.42$  to  $4.01$  indicated an acidic environment, and the temporal trends in RH, inorganic ions and  $H^+$  (aq) in aerosols are shown in Fig. S5. The oxidation of glyoxal and glyoxylic

acid by  $\bullet OH$  has been identified as an important pathway of oxalic acid production by field and laboratory studies (Ervens et al., 2004; Ervens and Volkamer, 2010; Wang et al., 2012, 2015). In summer, strong photochemical activity and high  $O_3$  concentrations in the afternoon lead to more production of dicarbonyls and aldehydes (e.g., glyoxal and methylglyoxal) from VOCs (Myriokefalitakis et al., 2011), which increases the precursors of oxalic acid. The aqueous-phase oxidation of glyoxal can take place in both clouds and wet aerosols (Lim et al., 2010). However, the lower yield of oxalic acid from glyoxal in wet aerosols compared to in clouds has been reported in previous chamber experiments due to the formation of a substantial amount of high-molecular-weight products such as oligomers in aerosol-related concentrations (Carlton et al., 2007; Tan et al., 2009). These findings may explain the lower peak of oxalic acid particles at 15:00 compared to that at 19:00. In addition, the precursors of oxalic acid such



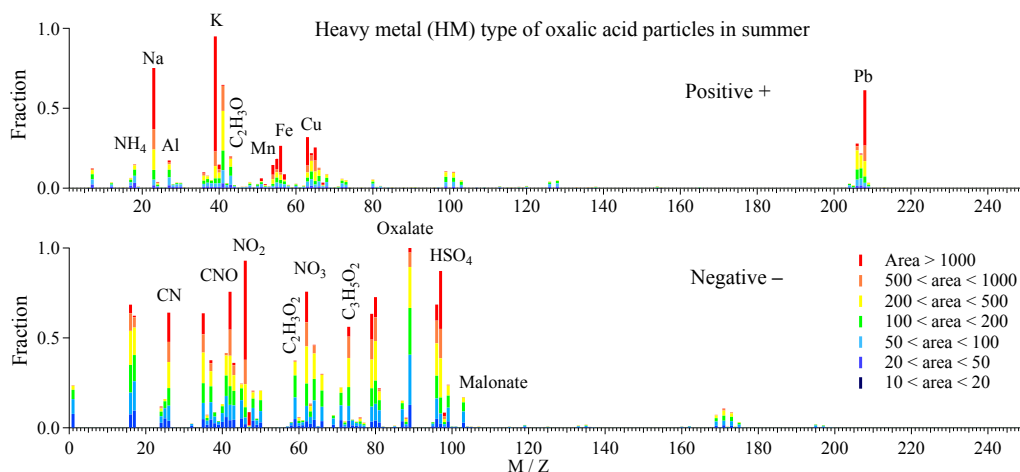


**Figure 6.** The averaged digitized positive and negative ion mass spectra of heavy metal oxalic-acid-containing particles in summer.

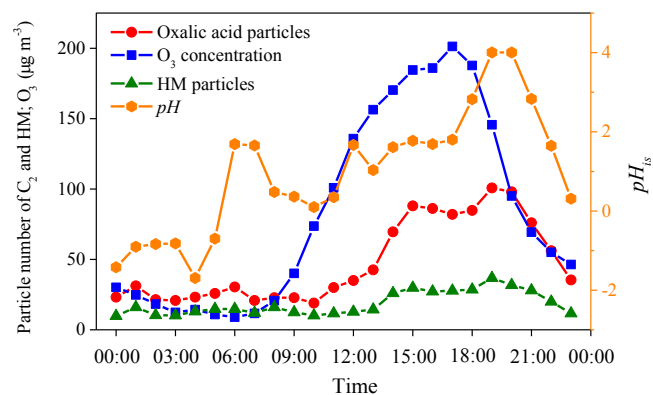


**Figure 7.** The diurnal variations in  $O_3$  concentration, oxalic acid particles, HM group particles and in situ pH ( $pH_{is}$ ) from 28 July to 1 August in 2014.

as glyoxylic acid have a higher reaction rate with  $\bullet OH$  in high-pH solutions according to previous studies (Ervens et al., 2003; Herrmann, 2003; Cheng et al., 2015), and in this work the increase in  $pH_{is}$  was observed as the enhancement of oxalic acid particles in the afternoon (Fig. 7), which suggests an efficient oxalic acid production from the oxidation of precursors.

The photochemical pattern of HM particles similar to  $O_3$  and total oxalic acid particles implies a possible participation of metal ions in the formation process of oxalic acid. The modeling studies from Ervens et al. (2014) suggest that oxalic acid production from glyoxal and glyoxylic acid in the aqueous phase significantly depends on  $\bullet OH$  availability (Ervens et al., 2014). The main sources of aqueous-phase  $\bullet OH$  in cloud droplets include direct uptake from the gas phase (Jacob, 1986), ozone photolysis by UV and visible light at the air–water interface (Anglada et al., 2014) and also aqueous-phase chemical reactions (Gligorovski et al., 2015).

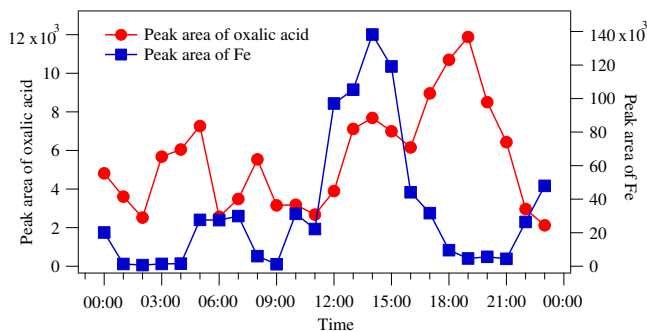


**Figure 8.** The diurnal variations in peak area of iron ( $m/z = 56$ ) and oxalic acid ( $m/z = -89$ ) in the HM oxalic acid particles from 28 July to 1 August 2014.

For the last kind of source,  $\bullet OH$  radicals could be generated through Fenton or Fenton-like reactions and photolysis of  $H_2O_2$ ,  $NO_3^-$ ,  $NO_2^-$  and chromophoric dissolved organic matter (CDOM) (Badali et al., 2015; Ervens, 2015; Herrmann et al., 2015; Tong et al., 2016). Given that the SPAMS cannot be used to quantify the concentrations of iron ions and  $H_2O_2$ , we will investigate the relative contribution of different source  $\bullet OH$  radicals to the formation of oxalic acid and show results in our follow-up studies.

The oxalic acid loss through the photolysis of iron oxalato complexes is a significant sink according to field measurements and model simulations (Sorooshian et al., 2013; Weller et al., 2014; Zhou et al., 2015). Considering the high abundance of iron in oxalic acid particles in the current work (Fig. 6), the photolysis of iron oxalato complexes could have played an important role in the diurnal variation in oxalic acid particles. Because the mass concentration of Fe (III) and oxalic acid could not be obtained using a SPAMS, the diurnal variations in peak area of iron ( $m/z = 56$ ) and oxalic acid ( $m/z = -89$ ) were used to investigate the role of



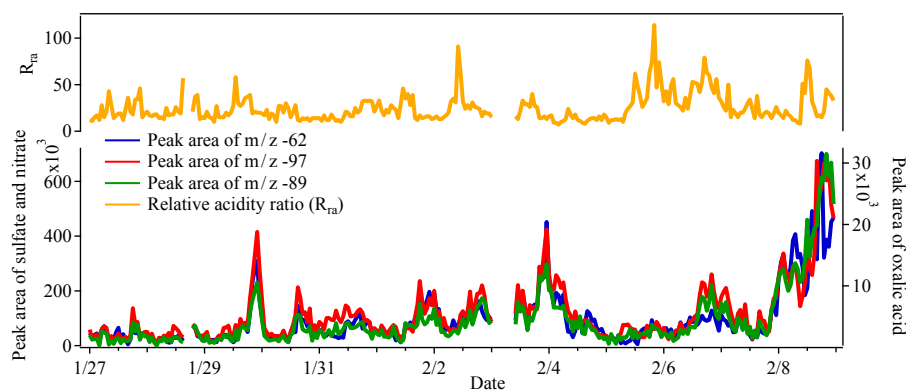


**Figure 9.** The temporal variations in peak area of nitrate, sulfate, and oxalic acid and the relative acidity ratio ( $R_{ra}$ ) in carbonaceous oxalic acid particles in winter.

iron in the net production of oxalic acid in the HM particles from 28 July to 1 August 2014 (Fig. 8). Interestingly, the peak area of iron exhibited opposite trends to the peak area of oxalic acid from 04:00 to 11:00. As the peak area of Fe increased from 1565 to 29 920 from 04:00 to 07:00, the peak area of oxalic acid decreased from 6052 to 3487 accordingly. From 08:00 to 11:00, the peak area of Fe had a very low value of 1168, but the peak area of oxalic had a very high value of 5538. In addition, the peak area of iron exhibited a high value of 138 199 at 14:00, while the peak area of oxalic acid showed a lower peak of 7687 at 14:00 and a higher peak of 11 879 at 19:00 with an extremely low abundance of iron. Above opposite variation patterns of iron and oxalic acid in iron-rich HM particles during the photochemical activity period from 05:00 to 19:00 strongly indicated that photolysis of iron oxalato complexes could be an efficient sink of oxalic acid.

The influence from traffic emissions was investigated through the diurnal variations in total EC particles and  $\text{NO}_2$  (Fig. S6). The EC particles increased from 12:00 to 21:00, which had the same variation as total oxalic acid, but  $\text{NO}_2$  followed the rush hour pattern, with two peaks from 05:00 to 08:00 and from 18:00 to 21:00. Traffic emission is not expected to have a large contribution to oxalic acid in this study. The wind speed was low during the whole day (Fig. S6), especially between 09:00 and 18:00, which provided a stagnant environment for the increase in oxalic acid produced from photochemical processes.

### 3.3 Formation process of oxalic acid in winter

Despite lower  $\text{O}_3$  concentrations and photochemical activity in winter, oxalic acid was still prevalent in carbonaceous particles, especially BB particles. While oxalic acid was found to be internally mixed with sulfate and nitrate both in summer and winter, the nitric acid was only observed in oxalic acid particles in winter, indicating a strongly acidic nature of oxalic acid particles in winter. Considering a possible connec-

tion of oxalic acid production with the acidic environment, the temporal concentrations of oxalic acid, sulfate and nitrate were investigated through their peak areas in the carbonaceous type oxalic acid particles, including EC, OC, ECOC and BB types in Fig. 9. The peaks of  $m/z$  -62 [ $\text{NO}_3^-$ ] and -97 [ $\text{HSO}_4^-$ ] represent nitrate and sulfate, respectively. Nitrate, sulfate and oxalic acid showed very similar variation patterns in winter, suggesting a close connection of the formation of oxalic acid with the existence of nitrate and sulfate. Although nitric acid was found in the oxalic acid particles, the acidity of the oxalic acid particles was not estimated since the real-time concentration of inorganic ions was not available during the sampling period in winter. Instead, the relative acidity ratio ( $R_{ra}$ ), defined as the ratio of total peak areas of nitrate and sulfate to the peak area of ammonium ( $m/z$  18 [ $\text{NH}_4^+$ ]), was used (Denkenberger et al., 2007; Pratt et al., 2009). The  $R_{ra}$  of carbonaceous type oxalic acid particles ranged from 7 to 114, with an average value of 25 (Fig. 9), indicating an intensely acidic environment of carbonaceous type oxalic acid particles in winter. Several studies have reported the formation of oxalic acid through the oxidation of glyoxal and related precursors in the acidic aqueous phase (Carlton et al., 2006, 2007; Tan et al., 2009). Although the influence of different particle acidity on the oxidation process of glyoxal still needs evaluation, the moderate acidic environment is favorable for the production of oxalic acid from the oxidation of glyoxal (Herrmann, 2003; Ervens and Volkamer, 2010; Eugene et al., 2016). In this work the acidic environment of the carbonaceous type oxalic acid particles and similar variation patterns among oxalic acid, sulfate and nitrate may suggest a relationship between the degradation of organic precursors and the acidic chemical process. However, the temporal change in  $R_{ra}$  did not follow a similar trend as the peak area of oxalic acid in most particles, possibly due to the multistep formation of oxalic acid influenced by many factors such as precursors, liquid water content and ion strength (Carlton et al., 2007; Cheng et al., 2013, 2015).

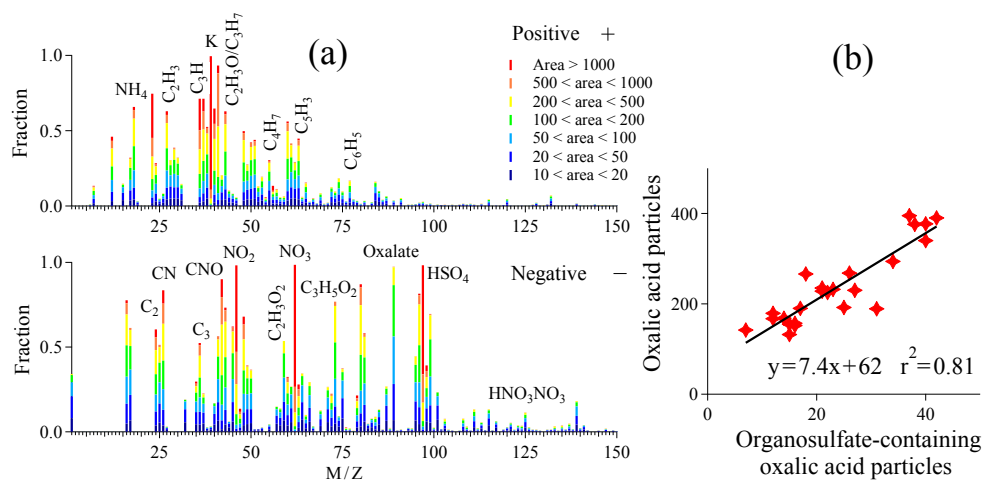


**Figure 10.** The comprehensive study of oxalic acid particle increase on 8 February 2015: **(a)** the digitized positive and negative ion mass spectrum of oxalic acid particles during the haze episode; **(b)** linear regression between total oxalic acid particles and organosulfate-containing oxalic acid particles ( $m/z \sim 155$ ).

**Table 2.** The abundance of major particle types in total oxalic-acid-containing particles during the haze episode in winter (8 February 2015).

	EC	ECOC	OC	BB	Sec	HM	Dust	Other
Count	1250	604	326	1320	856	377	814	132
Percentage, %	22.0	10.6	5.7	23.2	15.1	6.6	14.3	2.3

The sharp increase in oxalic acid particles on 8 February 2015 (Fig. 1) was selected as a typical haze episode to investigate the formation processes of oxalic acid in winter. During the haze episode, the 48 h back trajectory analysis showed air masses that originated from the urban areas of Guangzhou and Foshan cities (Fig. S4), indicating strong influence on organic precursors from anthropogenic emissions. Oxalic acid particle types were dominated by BB (23.2 %), followed by EC (22.0 %) and Sec (15.1 %) (Table 2). Carbonaceous particles including EC, ECOC, OC and BB accounted for 61.6 % of the total oxalic acid particles. The mass spectra of oxalic acid particles were characterized by many hydrocarbon clusters of  $27[\text{C}_2\text{H}_3]^+$ ,  $29[\text{C}_2\text{H}_5]^+$ ,  $37[\text{C}_3\text{H}]^+$ ,  $43[\text{C}_2\text{H}_3\text{O}]^+$ ,  $51[\text{C}_4\text{H}_3]^+$ ,  $55[\text{C}_4\text{H}_7]^+$ ,  $63[\text{C}_5\text{H}_3]^+$ ,  $65[\text{C}_5\text{H}_5]^+$ ,  $74[\text{C}_2\text{H}_2\text{O}_3]^+$ , and  $77[\text{C}_6\text{H}_5]^+$ , and carbon clusters of  $36[\text{C}_3]^+$ ,  $48[\text{C}_4]^+$ , and  $60[\text{C}_5]^+$  on a positive mass spectrum, while the negative mass spectrum was characterized by elemental carbon clusters like  $-24[\text{C}_2]^-$ ,  $-36[\text{C}_3]^-$ , and  $-48[\text{C}_4]^-$ ; biomass burning markers of  $-59[\text{C}_2\text{H}_3\text{O}_2]^-$  and  $-73[\text{C}_3\text{H}_5\text{O}_2]^-$ ; and secondary species including  $-42[\text{CNO}]^-$ ,  $-46[\text{NO}_2]^-$ ,  $-62[\text{NO}_3]^-$ ,  $-79[\text{PO}_3]^-$ ,  $-80[\text{SO}_3]^-$ ,  $-96[\text{SO}_4]^-$ , and  $-97[\text{HSO}_4]^-$  (Fig. 10a).

As the precursor of oxalic acid, glyoxal has the potential to react with sulfuric acid to produce organosulfates through acid-catalyzed nucleophilic addition according to laboratory and chamber studies (Surratt et al., 2007; Galloway et al., 2009). The negative ion of  $-155[\text{C}_2\text{H}_3\text{O}_2\text{SO}_4]^-$  has been identified as the marker ion of organosulfates derived from glyoxal in chamber and field measurements using ATOFMS (Surratt et al., 2008; Hatch et al., 2011). The formation of organosulfates from glyoxal requires an acidic aqueous environment, which can be used as a marker of the acidic aqueous-phase aging process of organic compounds. The temporal trend of organosulfate-containing oxalic acid particles in winter is shown in Fig. S7, which exhibited a similar pattern to the total oxalic acid particles during the whole sampling period in winter. The percentage of organosulfate-containing oxalic acid particles in total oxalic acid particles ranged from 0 to 16.4 %, with the highest ratio observed in the haze episode (8 February). The linear regression between total oxalic acid particles and organosulfate-containing oxalic acid particles in the haze episode is exhibited in Fig. 10b, and the robust correlation ( $r^2 = 0.81$ ) between them suggests that oxalic acid and organosulfate may share similar formation processes. Based on the discussion above, the degradation of carbonaceous species associated with acidic aqueous-phase chemical reactions may have an important contribution to the formation of oxalic acid during the haze episode in winter. Similar particle types and mass spectra of oxalic-acid-containing particles during the haze episode and the whole sampling period in winter were observed, which suggests the acidic aqueous-phase chemical processing of organic precursors as a potential source for oxalic acid.

#### 4 Summary and conclusions

Oxalic acid containing particles were measured using a single-particle aerosol mass spectrometer in the summer and winter of 2014 in Heshan, China. They accounted for 2.5 and 2.7 % of the total detected ambient particles. In summer, heavy-metal-containing particles were the largest group of particles containing oxalic acid, with a fraction of 31.3 %, followed by the Sec type (19.2 %), while in winter the BB type was the dominant group with a percentage of 24.2 %. More than 90 % of oxalic acid particles were internally mixed with sulfate and nitrate during the whole sampling period. Only 18 % of oxalic acid particles contained ammonium in summer, which increased to 71 % in winter. In summer, oxalic acid and O<sub>3</sub> concentration exhibited similar diurnal variations, indicating a substantial contribution of photochemical reactions to oxalic acid formation. The diurnal variations in peak area of iron and oxalic acid in HM particles indicate a net production of oxalic acid at 15:00 lower than at 19:00, likely due to a significant loss of oxalic acid through the photolysis of iron oxalato complexes during the strong photochemical activity period. In winter, carbonaceous particles, including EC, OC, ECOC and BB groups, accounted for 59.8 % of oxalic acid particles and increased to 61.6 % in the haze episode. Nitric acid and organosulfate were found to coexist in oxalic-acid-containing particles in the winter, which suggests a close association with acidic aqueous-phase reactions. Acidic aqueous-phase chemical processing of organic precursors is a potential contribution for the formation of oxalic acid in winter. The current study demonstrates that the SPAMS is a unique tool for understanding the mixing states of different components of ambient aerosols, which are useful for exploring the formation and evolution process of SOA.

**Data availability.** The observational data including SPAMS, meteorological parameters and inorganic ions used in this study are available from corresponding authors upon request (limei2007@163.com).

**The Supplement related to this article is available online at <https://doi.org/10.5194/acp-17-9519-2017-supplement>.**

**Competing interests.** Zhong Fu and Yanru Bi are both employees at Guangzhou Hexin Analytical Instrument Limited Company.

**Acknowledgements.** This work was financially supported by the National Key Technology R&D Program (grant no. 2014BAC21B01), the Guangdong Province Public Interest Research and Capacity Building Special Fund (grant no.

2014B020216005), the Strategic Priority Research Program (B) of the Chinese Academy of Sciences (grant no. XDB05040502), the Guangdong Industry–University Research Program (grant no. 2012B090500014), and the NSFC of Guangdong Province (grant no. 2015A030313339). Chak K. Chan would like to acknowledge funding support of the General Fund of National Natural Science Foundation of China (grant no. 41675117). Haijie Tong acknowledges the Max Planck Society for funding and Ulrich Pöschl for helpful discussions.

Edited by: Kimitaka Kawamura

Reviewed by: three anonymous referees

#### References

- Aggarwal, S. G. and Kawamura, K.: Molecular distributions and stable carbon isotopic compositions of dicarboxylic acids and related compounds in aerosols from Sapporo, Japan: Implications for photochemical aging during long-range atmospheric transport, *J. Geophys. Res.-Atmos.*, 113, D14301, <https://doi.org/10.1029/2007jd009365>, 2008.
- Anglada, J. M., Martins-Costa, M., Ruiz-López, M. F., and Francisco, J. S.: Spectroscopic signatures of ozone at the air–water interface and photochemistry implications, *P. Natl. Acad. Sci. USA*, 111, 11618–11623, <https://doi.org/10.1073/pnas.1411727111>, 2014.
- Badali, K. M., Zhou, S., Aljawhary, D., Antiñolo, M., Chen, W. J., Lok, A., Mungall, E., Wong, J. P. S., Zhao, R., and Abbatt, J. P. D.: Formation of hydroxyl radicals from photolysis of secondary organic aerosol material, *Atmos. Chem. Phys.*, 15, 7831–7840, <https://doi.org/10.5194/acp-15-7831-2015>, 2015.
- Behera, S. N., Betha, R., Liu, P., and Balasubramanian, R.: A study of diurnal variations of PM<sub>2.5</sub> acidity and related chemical species using a new thermodynamic equilibrium model, *Sci. Total Environ.*, 452, 286–295, 2013.
- Bi, X., Zhang, G., Li, L., Wang, X., Li, M., Sheng, G., Fu, J., and Zhou, Z.: Mixing state of biomass burning particles by single particle aerosol mass spectrometer in the urban area of PRD, China, *Atmos. Environ.*, 45, 3447–3453, 2011.
- Booth, A. M., Topping, D. O., McFiggans, G., and Percival, C. J.: Surface tension of mixed inorganic and dicarboxylic acid aqueous solutions at 298.15 K and their importance for cloud activation predictions, *Phys. Chem. Chem. Phys.*, 11, 8021–8028, <https://doi.org/10.1039/b906849j>, 2009.
- Carlton, A. G., Turpin, B. J., Lim, H. J., Altieri, K. E., and Seitzinger, S.: Link between isoprene and secondary organic aerosol (SOA): Pyruvic acid oxidation yields low volatility organic acids in clouds, *Geophys. Res. Lett.*, 33, L06822, <https://doi.org/10.1029/2005gl025374>, 2006.
- Carlton, A. G., Turpin, B. J., Altieri, K. E., Seitzinger, S., Reff, A., Lim, H. J., and Ervens, B.: Atmospheric oxalic acid and SOA production from glyoxal: Results of aqueous photooxidation experiments, *Atmos. Environ.*, 41, 7588–7602, <https://doi.org/10.1016/j.atmosenv.2007.05.035>, 2007.
- Cheng, C., Wang, G., Meng, J., Wang, Q., Cao, J., Li, J., and Wang, J.: Size-resolved airborne particulate oxalic and related secondary organic aerosol species in the urban atmosphere of Chengdu, China, *Atmos. Res.*, 161, 134–142, 2015.

- Cheng, C. L., Wang, G. H., Zhou, B. H., Meng, J. J., Li, J. J., Cao, J. J., and Xiao, S.: Comparison of dicarboxylic acids and related compounds in aerosol samples collected in Xi'an, China during haze and clean periods, *Atmos. Environ.*, 81, 443–449, <https://doi.org/10.1016/j.atmosenv.2013.09.013>, 2013.
- Denkenberger, K. A., Moffet, R. C., Holecek, J. C., Rebotier, T. P., and Prather, K. A.: Real-time, single-particle measurements of oligomers in aged ambient aerosol particles, *Environ. Sci. Technol.*, 41, 5439–5446, <https://doi.org/10.1021/es070329l>, 2007.
- Du, H., Kong, L., Cheng, T., Chen, J., Du, J., Li, L., Xia, X., Leng, C., and Huang, G.: Insights into summertime haze pollution events over Shanghai based on online water-soluble ionic composition of aerosols, *Atmos. Environ.*, 45, 5131–5137, 2011.
- Ervens, B.: Modeling the Processing of Aerosol and Trace Gases in Clouds and Fogs, *Chem. Rev.*, 115, 4157–4198, <https://doi.org/10.1021/cr5005887>, 2015.
- Ervens, B. and Volkamer, R.: Glyoxal processing by aerosol multiphase chemistry: towards a kinetic modeling framework of secondary organic aerosol formation in aqueous particles, *Atmos. Chem. Phys.*, 10, 8219–8244, <https://doi.org/10.5194/acp-10-8219-2010>, 2010.
- Ervens, B., Gligorovski, S., and Herrmann, H.: Temperature-dependent rate constants for hydroxyl radical reactions with organic compounds in aqueous solutions, *Phys. Chem. Chem. Phys.*, 5, 1811–1824, <https://doi.org/10.1039/B300072a>, 2003.
- Ervens, B., Feingold, G., Frost, G. J., and Kreidenweis, S. M.: A modeling study of aqueous production of dicarboxylic acids: 1. Chemical pathways and speciated organic mass production, *J. Geophys. Res.-Atmos.*, 109, D15205, <https://doi.org/10.1029/2003jd004387>, 2004.
- Ervens, B., Turpin, B. J., and Weber, R. J.: Secondary organic aerosol formation in cloud droplets and aqueous particles (aqSOA): a review of laboratory, field and model studies, *Atmos. Chem. Phys.*, 11, 11069–11102, <https://doi.org/10.5194/acp-11-11069-2011>, 2011.
- Ervens, B., Sorooshian, A., Lim, Y. B., and Turpin, B. J.: Key parameters controlling OH-initiated formation of secondary organic aerosol in the aqueous phase (aqSOA), *J. Geophys. Res.-Atmos.*, 119, 3997–4016, <https://doi.org/10.1002/2013jd021021>, 2014.
- Eugene, A. J., Xia, S. S., and Guzman, M. I.: Aqueous Photochemistry of Glyoxylic Acid, *J. Phys. Chem. A*, 120, 3817–3826, <https://doi.org/10.1021/acs.jpca.6b00225>, 2016.
- Fountoukis, C. and Nenes, A.: ISORROPIA II: a computationally efficient thermodynamic equilibrium model for  $K^+$ – $Ca^{2+}$ – $Mg^{2+}$ – $NH_4^+$ – $Na^+$ – $SO_4^{2-}$ – $NO_3^-$ – $Cl^-$ – $H_2O$  aerosols, *Atmos. Chem. Phys.*, 7, 4639–4659, <https://doi.org/10.5194/acp-7-4639-2007>, 2007.
- Galloway, M. M., Chhabra, P. S., Chan, A. W. H., Surratt, J. D., Flagan, R. C., Seinfeld, J. H., and Keutsch, F. N.: Glyoxal uptake on ammonium sulphate seed aerosol: reaction products and reversibility of uptake under dark and irradiated conditions, *Atmos. Chem. Phys.*, 9, 3331–3345, <https://doi.org/10.5194/acp-9-3331-2009>, 2009.
- Gligorovski, S., Strekowski, R., Barbati, S., and Vione, D.: Environmental Implications of Hydroxyl Radicals (OH), *Chem. Rev.*, 115, 13051–13092, [10.1021/cr500310b](https://doi.org/10.1021/cr500310b), 2015.
- Goldstein, A. H. and Galbally, I. E.: Known and unexplored organic constituents in the earth's atmosphere, *Environ. Sci. Technol.*, 41, 1514–1521, <https://doi.org/10.1021/Es072476p>, 2007.
- Hallquist, M., Wenger, J. C., Baltensperger, U., Rudich, Y., Simpson, D., Claeys, M., Dommen, J., Donahue, N. M., George, C., Goldstein, A. H., Hamilton, J. F., Herrmann, H., Hoffmann, T., Iinuma, Y., Jang, M., Jenkin, M. E., Jimenez, J. L., Kiendler-Scharr, A., Maenhaut, W., McFiggans, G., Mentel, Th. F., Monod, A., Prévôt, A. S. H., Seinfeld, J. H., Surratt, J. D., Szmigielski, R., and Wildt, J.: The formation, properties and impact of secondary organic aerosol: current and emerging issues, *Atmos. Chem. Phys.*, 9, 5155–5236, <https://doi.org/10.5194/acp-9-5155-2009>, 2009.
- Hatch, L. E., Creamean, J. M., Ault, A. P., Surratt, J. D., Chan, M. N., Seinfeld, J. H., Edgerton, E. S., Su, Y., and Prather, K. A.: Measurements of isoprene-derived organosulfates in ambient aerosols by aerosol time-of-flight mass spectrometry-Part 1: Single particle atmospheric observations in Atlanta, *Environ. Sci. Technol.*, 45, 5105–5111, 2011.
- Herrmann, H.: Kinetics of aqueous phase reactions relevant for atmospheric chemistry, *Chem. Rev.*, 103, 4691–4716, <https://doi.org/10.1021/Cr020658q>, 2003.
- Herrmann, H., Schaefer, T., Tilgner, A., Styler, S. A., Weller, C., Teich, M., and Otto, T.: Tropospheric Aqueous-Phase Chemistry: Kinetics, Mechanisms, and Its Coupling to a Changing Gas Phase, *Chem. Rev.*, 115, 4259–4334, <https://doi.org/10.1021/cr500447k>, 2015.
- Ho, K. F., Cao, J. J., Lee, S. C., Kawamura, K., Zhang, R. J., Chow, J. C., and Watson, J. G.: Dicarboxylic acids, ketocarboxylic acids, and dicarbonyls in the urban atmosphere of China, *J. Geophys. Res.-Atmos.*, 112, D22S27, <https://doi.org/10.1029/2006jd008011>, 2007.
- Ho, K. F., Lee, S. C., Ho, S. S. H., Kawamura, K., Tachibana, E., Cheng, Y., and Zhu, T.: Dicarboxylic acids, ketocarboxylic acids, alpha-dicarbonyls, fatty acids, and benzoic acid in urban aerosols collected during the 2006 Campaign of Air Quality Research in Beijing (CAREBeijing-2006), *J. Geophys. Res.-Atmos.*, 115, D19312, <https://doi.org/10.1029/2009jd013304>, 2010.
- Ho, K. F., Ho, S. S. H., Lee, S. C., Kawamura, K., Zou, S. C., Cao, J. J., and Xu, H. M.: Summer and winter variations of dicarboxylic acids, fatty acids and benzoic acid in PM<sub>2.5</sub> in Pearl Delta River Region, China, *Atmos. Chem. Phys.*, 11, 2197–2208, <https://doi.org/10.5194/acp-11-2197-2011>, 2011.
- Huang, X.-F. and Yu, J. Z.: Is vehicle exhaust a significant primary source of oxalic acid in ambient aerosols?, *Geophys. Res. Lett.*, 34, L02808, <https://doi.org/10.1029/2006gl028457>, 2007.
- Jacob, D. J.: Chemistry of OH in remote clouds and its role in the production of formic acid and peroxy-monosulfate, *J. Geophys. Res.-Atmos.*, 91, 9807–9826, <https://doi.org/10.1029/JD091iD09p09807>, 1986.
- Jimenez, J. L., Canagaratna, M. R., Donahue, N. M., Prevot, A. S. H., Zhang, Q., Kroll, J. H., DeCarlo, P. F., Allan, J. D., Coe, H., Ng, N. L., Aiken, A. C., Docherty, K. S., Ulbrich, I. M., Grieshop, A. P., Robinson, A. L., Duplissy, J., Smith, J. D., Wilson, K. R., Lanz, V. A., Hueglin, C., Sun, Y. L., Tian, J., Laaksonen, A., Raatikainen, T., Rautiainen, J., Vaattovaara, P., Ehn, M., Kulmala, M., Tomlinson, J. M., Collins, D. R., Cubison, M. J., Dunlea, E. J., Huffman, J. A., Onasch, T. B., Alfarra, M. R., Williams, P. I., Bower, K., Kondo, Y., Schneider, J., Drewnick,

- F., Borrmann, S., Weimer, S., Demerjian, K., Salcedo, D., Cottrell, L., Griffin, R., Takami, A., Miyoshi, T., Hatakeyama, S., Shimono, A., Sun, J. Y., Zhang, Y. M., Dzepina, K., Kimmel, J. R., Sueper, D., Jayne, J. T., Herndon, S. C., Trimborn, A. M., Williams, L. R., Wood, E. C., Middlebrook, A. M., Kolb, C. E., Baltensperger, U., and Worsnop, D. R.: Evolution of Organic Aerosols in the Atmosphere, *Science*, 326, 1525–1529, <https://doi.org/10.1126/science.1180353>, 2009.
- Kawamura, K. and Ikushima, K.: seasonal-changes in the distribution of dicarboxylic-acids in the urban atmosphere, *Environ. Sci. Technol.*, 27, 2227–2235, <https://doi.org/10.1021/es00047a033>, 1993.
- Kawamura, K. and Yasui, O.: Diurnal changes in the distribution of dicarboxylic acids, ketocarboxylic acids and dicarbonyls in the urban Tokyo atmosphere, *Atmos. Environ.*, 39, 1945–1960, <https://doi.org/10.1016/j.atmosenv.2004.12.014>, 2005.
- Kawamura, K., Kobayashi, M., Tsubonuma, N., Mochida, M., Watanabe, T., and Lee, M.: Organic and inorganic compositions of marine aerosols from East Asia: Seasonal variations of water-soluble dicarboxylic acids, major ions, total carbon and nitrogen, and stable C and N isotopic composition, *Geochemical Investigations in Earth and Space Science: A Tribute to Issac R. Kaplan*, *Geo. Soc. S. P.*, 9, 243–265, [https://doi.org/10.1016/S1873-9881\(04\)80019-1](https://doi.org/10.1016/S1873-9881(04)80019-1), 2004.
- Kawamura, K., Kasukabe, H., and Barrie, L. A.: Secondary formation of water-soluble organic acids and alpha-dicarbonyls and their contributions to total carbon and water-soluble organic carbon: Photochemical aging of organic aerosols in the Arctic spring, *J. Geophys. Res.-Atmos.*, 115, D21306, <https://doi.org/10.1029/2010jd014299>, 2010.
- Kawamura, K., Tachibana, E., Okuzawa, K., Aggarwal, S. G., Kanaya, Y., and Wang, Z. F.: High abundances of water-soluble dicarboxylic acids, ketocarboxylic acids and a-dicarbonyls in the mountaintop aerosols over the North China Plain during wheat burning season, *Atmos. Chem. Phys.*, 13, 8285–8302, <https://doi.org/10.5194/acp-13-8285-2013>, 2013.
- Khezri, B., Mo, H., Yan, Z., Chong, S.-L., Heng, A. K., and Webster, R. D.: Simultaneous online monitoring of inorganic compounds in aerosols and gases in an industrialized area, *Atmos. Environ.*, 80, 352–360, 2013.
- Kundu, S., Kawamura, K., Andreae, T. W., Hoffer, A., and Andreae, M. O.: Molecular distributions of dicarboxylic acids, ketocarboxylic acids and a-dicarbonyls in biomass burning aerosols: implications for photochemical production and degradation in smoke layers, *Atmos. Chem. Phys.*, 10, 2209–2225, <https://doi.org/10.5194/acp-10-2209-2010>, 2010.
- Li, L., Huang, Z. X., Dong, J. G., Li, M., Gao, W., Nian, H. Q., Fu, Z., Zhang, G. H., Bi, X. H., Cheng, P., and Zhou, Z.: Real time bipolar time-of-flight mass spectrometer for analyzing single aerosol particles, *Int. J. Mass. Spectrom.*, 303, 118–124, <https://doi.org/10.1016/j.ijms.2011.01.017>, 2011.
- Li, L., Li, M., Huang, Z., Gao, W., Nian, H., Fu, Z., Gao, J., Chai, F., and Zhou, Z.: Ambient particle characterization by single particle aerosol mass spectrometry in an urban area of Beijing, *Atmos. Environ.*, 94, 323–331, 2014.
- Lim, Y. B., Tan, Y., Perri, M. J., Seitzinger, S. P., and Turpin, B. J.: Aqueous chemistry and its role in secondary organic aerosol (SOA) formation, *Atmos. Chem. Phys.*, 10, 10521–10539, <https://doi.org/10.5194/acp-10-10521-2010>, 2010.
- Ma, Q. X., He, H., and Liu, C.: Hygroscopic properties of oxalic acid and atmospherically relevant oxalates, *Atmos. Environ.*, 69, 281–288, <https://doi.org/10.1016/j.atmosenv.2012.12.011>, 2013.
- McNeill, V. F.: Aqueous organic chemistry in the atmosphere: Sources and chemical processing of organic aerosols, *Environ. Sci. Technol.*, 49, 1237–1244, 2015.
- Meng, J. J., Wang, G. H., Li, J. J., Cheng, C. L., and Cao, J. J.: Atmospheric oxalic acid and related secondary organic aerosols in Qinghai Lake, a continental background site in Tibet Plateau, *Atmos. Environ.*, 79, 582–589, <https://doi.org/10.1016/j.atmosenv.2013.07.024>, 2013.
- Meng, J. J., Wang, G. H., Li, J. J., Cheng, C. L., Ren, Y. Q., Huang, Y., Cheng, Y. T., Cao, J. J., and Zhang, T.: Seasonal characteristics of oxalic acid and related SOA in the free troposphere of Mt. Hua, central China: Implications for sources and formation mechanisms, *Sci. Total Environ.*, 493, 1088–1097, <https://doi.org/10.1016/j.scitotenv.2014.04.086>, 2014.
- Miyazaki, Y., Aggarwal, S. G., Singh, K., Gupta, P. K., and Kawamura, K.: Dicarboxylic acids and water-soluble organic carbon in aerosols in New Delhi, India, in winter: Characteristics and formation processes, *J. Geophys. Res.-Atmos.*, 114, D19206, <https://doi.org/10.1029/2009jd011790>, 2009.
- Myriokefalitakis, S., Tsigaridis, K., Mihalopoulos, N., Sciare, J., Nenes, A., Kawamura, K., Segers, A., and Kanakidou, M.: In-cloud oxalate formation in the global troposphere: a 3-D modeling study, *Atmos. Chem. Phys.*, 11, 5761–5782, <https://doi.org/10.5194/acp-11-5761-2011>, 2011.
- Nenes, A., Pandis, S. N., and Pilinis, C.: ISORROPIA: A new thermodynamic equilibrium model for multiphase multicomponent inorganic aerosols, *Aquat. Geochem.*, 4, 123–152, 1998.
- Nenes, A., Pandis, S. N., and Pilinis, C.: Continued development and testing of a new thermodynamic aerosol module for urban and regional air quality models, *Atmos. Environ.*, 33, 1553–1560, 1999.
- Noble, C. A. and Prather, K. A.: Real-time measurement of correlated size and composition profiles of individual atmospheric aerosol particles, *Environ. Sci. Technol.*, 30, 2667–2680, 1996.
- Novakov, T. and Penner, J. E.: Large Contribution of Organic Aerosols to Cloud-Condensation-Nuclei Concentrations, *Nature*, 365, 823–826, <https://doi.org/10.1038/365823a0>, 1993.
- Pavuluri, C. M., Kawamura, K., and Swaminathan, T.: Water-soluble organic carbon, dicarboxylic acids, ketoacids, and alpha-dicarbonyls in the tropical Indian aerosols, *J. Geophys. Res.-Atmos.*, 115, D11302, <https://doi.org/10.1029/2009JD012661>, 2010.
- Pöschl, U. and Shiraiwa, M.: Multiphase Chemistry at the Atmosphere-Biosphere Interface Influencing Climate and Public Health in the Anthropocene, *Chem. Rev.*, 115, 4440–4475, <https://doi.org/10.1021/cr500487s>, 2015.
- Prather, K. A., Nordmeyer, T., and Salt, K.: Real-time characterization of individual aerosol particles using time-of-flight mass spectrometry, *Anal. Chem.*, 66, 1403–1407, 1994.
- Pratt, K. A., Hatch, L. E., and Prather, K. A.: Seasonal Volatility Dependence of Ambient Particle Phase Amines, *Environ. Sci. Technol.*, 43, 5276–5281, <https://doi.org/10.1021/es803189n>, 2009.
- Prenni, A. J., De Mott, P. J., and Kreidenweis, S. M.: Water uptake of internally mixed particles containing ammonium sulfate and dicarboxylic acids, *Atmos. Environ.*, 37, 4243–4251, [https://doi.org/10.1016/s1352-2310\(03\)00559-4](https://doi.org/10.1016/s1352-2310(03)00559-4), 2003.

- Silva, P. J. and Prather, K. A.: Interpretation of mass spectra from organic compounds in aerosol time-of-flight mass spectrometry, *Anal. Chem.*, 72, 3553–3562, 2000.
- Sorooshian, A., Varutbangkul, V., Brechtel, F. J., Ervens, B., Feingold, G., Bahreini, R., Murphy, S. M., Holloway, J. S., Atlas, E. L., Buzorius, G., Jonsson, H., Flagan, R. C., and Seinfeld, J. H.: Oxalic acid in clear and cloudy atmospheres: Analysis of data from International Consortium for Atmospheric Research on Transport and Transformation 2004, *J. Geophys. Res.-Atmos.*, 111, D23S45, <https://doi.org/10.1029/2005jd006880>, 2006.
- Sorooshian, A., Lu, M.-L., Brechtel, F. J., Jonsson, H., Feingold, G., Flagan, R. C., and Seinfeld, J. H.: On the source of organic acid aerosol layers above clouds, *Environ. Sci. Technol.*, 41, 4647–4654, <https://doi.org/10.1021/es0630442>, 2007a.
- Sorooshian, A., Ng, N. L., Chan, A. W. H., Feingold, G., Flagan, R. C., and Seinfeld, J. H.: Particulate organic acids and overall water-soluble aerosol composition measurements from the 2006 Gulf of Mexico Atmospheric Composition and Climate Study (GoMACCS), *J. Geophys. Res.-Atmos.*, 112, D13201, <https://doi.org/10.1029/2007jd008537>, 2007b.
- Sorooshian, A., Wang, Z., Coggon, M. M., Jonsson, H. H., and Ervens, B.: Observations of Sharp Oxalate Reductions in Stratocumulus Clouds at Variable Altitudes: Organic Acid and Metal Measurements During the 2011 E-PEACE Campaign, *Environ. Sci. Technol.*, 47, 7747–7756, <https://doi.org/10.1021/es4012383>, 2013.
- Stone, E. A., Hedman, C. J., Zhou, J. B., Mieritz, M., and Schauer, J. J.: Insights into the nature of secondary organic aerosol in Mexico City during the MILAGRO experiment 2006, *Atmos. Environ.*, 44, 312–319, <https://doi.org/10.1016/j.atmosenv.2009.10.036>, 2010.
- Sullivan, R. C. and Prather, K. A.: Investigations of the diurnal cycle and mixing state of oxalic acid in individual particles in Asian aerosol outflow, *Environ. Sci. Technol.*, 41, 8062–8069, <https://doi.org/10.1021/es071134g>, 2007.
- Surratt, J. D., Kroll, J. H., Kleindienst, T. E., Edney, E. O., Claeys, M., Sorooshian, A., Ng, N. L., Offenberg, J. H., Lewandowski, M., Jaoui, M., Flagan, R. C., and Seinfeld, J. H.: Evidence for organosulfates in secondary organic aerosol, *Environ. Sci. Technol.*, 41, 517–527, <https://doi.org/10.1021/Es062081q>, 2007.
- Surratt, J. D., Gomez-Gonzalez, Y., Chan, A. W. H., Vermeylen, R., Shahgholi, M., Kleindienst, T. E., Edney, E. O., Offenberg, J. H., Lewandowski, M., Jaoui, M., Maenhaut, W., Claeys, M., Flagan, R. C., and Seinfeld, J. H.: Organosulfate formation in biogenic secondary organic aerosol, *J. Phys. Chem. A*, 112, 8345–8378, <https://doi.org/10.1021/Jp802310p>, 2008.
- Tan, Y., Perri, M. J., Seitzinger, S. P., and Turpin, B. J.: Effects of Precursor Concentration and Acidic Sulfate in Aqueous Glyoxal-OH Radical Oxidation and Implications for Secondary Organic Aerosol, *Environ. Sci. Technol.*, 43, 8105–8112, <https://doi.org/10.1021/Es901742f>, 2009.
- ten Brink, H., Otjes, R., Jongejan, P., and Slanina, S.: An instrument for semi-continuous monitoring of the size-distribution of nitrate, ammonium, sulphate and chloride in aerosol, *Atmos. Environ.*, 41, 2768–2779, 2007.
- Tong, H., Arangio, A. M., Lakey, P. S. J., Berkemeier, T., Liu, F., Kampf, C. J., Brune, W. H., Pöschl, U., and Shiraiwa, M.: Hydroxyl radicals from secondary organic aerosol decomposition in water, *Atmos. Chem. Phys.*, 16, 1761–1771, <https://doi.org/10.5194/acp-16-1761-2016>, 2016.
- van Pinxteren, D., Neusüß, C., and Herrmann, H.: On the abundance and source contributions of dicarboxylic acids in size-resolved aerosol particles at continental sites in central Europe, *Atmos. Chem. Phys.*, 14, 3913–3928, <https://doi.org/10.5194/acp-14-3913-2014>, 2014.
- Wang, G., Kawamura, K., Cheng, C. L., Li, J. J., Cao, J. J., Zhang, R. J., Zhang, T., Liu, S. X., and Zhao, Z. Z.: Molecular Distribution and Stable Carbon Isotopic Composition of Dicarboxylic Acids, Ketocarboxylic Acids, and  $\alpha$ -Dicarbonyls in Size-Resolved Atmospheric Particles From Xi'an City, China, *Environ. Sci. Technol.*, 46, 4783–4791, <https://doi.org/10.1021/es204322c>, 2012.
- Wang, G., Cheng, C., Meng, J., Huang, Y., Li, J., and Ren, Y.: Field observation on secondary organic aerosols during Asian dust storm periods: Formation mechanism of oxalic acid and related compounds on dust surface, *Atmos. Environ.*, 113, 169–176, 2015.
- Wang, G., Zhang, R., Gomez, M. E., Yang, L., Levy Zamora, M., Hu, M., Lin, Y., Peng, J., Guo, S., Meng, J., Li, J., Cheng, C., Hu, T., Ren, Y., Wang, Y., Gao, J., Cao, J., An, Z., Zhou, W., Li, G., Wang, J., Tian, P., Marrero-Ortiz, W., Secrest, J., Du, Z., Zheng, J., Shang, D., Zeng, L., Shao, M., Wang, W., Huang, Y., Wang, Y., Zhu, Y., Li, Y., Hu, J., Pan, B., Cai, L., Cheng, Y., Ji, Y., Zhang, F., Rosenfeld, D., Liss, P. S., Duce, R. A., Kolb, C. E., and Molina, M. J.: Persistent sulfate formation from London Fog to Chinese haze, *P. Natl. Acad. Sci. USA*, 113, 13630–13635, <https://doi.org/10.1073/pnas.1616540113>, 2016.
- Wang, J., Wang, G., Gao, J., Wang, H., Ren, Y., Li, J., Zhou, B., Wu, C., Zhang, L., Wang, S., and Chai, F.: Concentrations and stable carbon isotope compositions of oxalic acid and related SOA in Beijing before, during, and after the 2014 APEC, *Atmos. Chem. Phys.*, 17, 981–992, <https://doi.org/10.5194/acp-17-981-2017>, 2017.
- Weller, C., Tilgner, A., Brauer, P., and Herrmann, H.: Modeling the Impact of Iron-Carboxylate Photochemistry on Radical Budget and Carboxylate Degradation in Cloud Droplets and Particles, *Environ. Sci. Technol.*, 48, 5652–5659, <https://doi.org/10.1021/es4056643>, 2014.
- Wonaschuetz, A., Sorooshian, A., Ervens, B., Chuang, P. Y., Feingold, G., Murphy, S. M., de Gouw, J., Warneke, C., and Jonsson, H. H.: Aerosol and gas re-distribution by shallow cumulus clouds: An investigation using airborne measurements, *J. Geophys. Res.-Atmos.*, 117, D17202, <https://doi.org/10.1029/2012jd018089>, 2012.
- Xue, J., Lau, A. K. H., and Yu, J. Z.: A study of acidity on PM<sub>2.5</sub> in Hong Kong using online ionic chemical composition measurements, *Atmos. Environ.*, 45, 7081–7088, <https://doi.org/10.1016/j.atmosenv.2011.09.040>, 2011.
- Yang, F., Chen, H., Wang, X., Yang, X., Du, J., and Chen, J.: Single particle mass spectrometry of oxalic acid in ambient aerosols in Shanghai: Mixing state and formation mechanism, *Atmos. Environ.*, 43, 3876–3882, 2009.
- Yao, X. H., Fang, M., and Chan, C. K.: Size distributions and formation of dicarboxylic acids in atmospheric particles, *Atmos. Environ.*, 36, 2099–2107, 2002.
- Yao, X. H., Lau, A. P. S., Fang, M., Chan, C. K., and Hu, M.: Size distributions and formation of ionic species in atmospheric

- particulate pollutants in Beijing, China: 2 – dicarboxylic acids, *Atmos. Environ.*, 37, 3001–3007, [https://doi.org/10.1016/s1352-2310\(03\)00256-5](https://doi.org/10.1016/s1352-2310(03)00256-5), 2003.
- Yu, J. Z., Huang, X. F., Xu, J. H., and Hu, M.: When aerosol sulfate goes up, so does oxalate: Implication for the formation mechanisms of oxalate, *Environ. Sci. Technol.*, 39, 128–133, <https://doi.org/10.1021/Es049559f>, 2005.
- Yu, L., Smith, J., Laskin, A., Anastasio, C., Laskin, J., and Zhang, Q.: Chemical characterization of SOA formed from aqueous-phase reactions of phenols with the triplet excited state of carbonyl and hydroxyl radical, *Atmos. Chem. Phys.*, 14, 13801–13816, <https://doi.org/10.5194/acp-14-13801-2014>, 2014.
- Zauscher, M. D., Wang, Y., Moore, M. J. K., Gaston, C. J., and Prather, K. A.: Air Quality Impact and Physicochemical Aging of Biomass Burning Aerosols during the 2007 San Diego Wildfires, *Environ. Sci. Technol.*, 47, 7633–7643, <https://doi.org/10.1021/es4004137>, 2013.
- Zhang, G., Bi, X., Li, L., Chan, L. Y., Li, M., Wang, X., Sheng, G., Fu, J., and Zhou, Z.: Mixing state of individual submicron carbon-containing particles during spring and fall seasons in urban Guangzhou, China: a case study, *Atmos. Chem. Phys.*, 13, 4723–4735, <https://doi.org/10.5194/acp-13-4723-2013>, 2013.
- Zhang, G., Bi, X., He, J., Chen, D., Chan, L. Y., Xie, G., Wang, X., Sheng, G., Fu, J., and Zhou, Z.: Variation of secondary coatings associated with elemental carbon by single particle analysis, *Atmos. Environ.*, 92, 162–170, 2014.
- Zhang, R., Wang, G., Guo, S., Zamora, M. L., Ying, Q., Lin, Y., Wang, W., Hu, M., and Wang, Y.: Formation of urban fine particulate matter, *Chem. Rev.*, 115, 3803–3855, 2015.
- Zhou, Y., Huang, X. H., Bian, Q., Griffith, S. M., Louie, P. K., and Yu, J. Z.: Sources and atmospheric processes impacting oxalate at a suburban coastal site in Hong Kong: Insights inferred from 1 year hourly measurements, *J. Geophys. Res.-Atmos.*, 120, 9772–9788, 2015.